Journal of Non-Oxide Glasses Vol. 9, No 3, 2017, p. 65 – 72

SYNTHESIS AND CHARACTERIZATION OF ENVIRONMENTALLY SAFE TIN MONO SULFIDE NANOMATERIALS FOR SUSTAINABLE SOLAR ENERGY CONVERSION

W. A. A. SYED[a], N. RAFIQ[a], M. A. GHUFRAN[b*], H. A. QURESHI[a], M. ZAMAN[a]
[a]*Department of Physics, International Islamic University, Islamabad, Pakistan 44000,*
[b]*Department of Environmental Science, International Islamic University, Islamabad, Pakistan* 44000

Nanoparticles of tin mono sulfide (SnS), an important and environmentally safe material for the application in optoelectronic devices, have been synthesized by the co-precipitation method. Structural, morphological and optical properties have been investigated with the help of x-ray diffraction technique (XRD), secondary electron microscope (SEM), diffuse reflectance spectroscopy and FTIR respectively. The phase and particle size, determined by XRD and SEM shows the uniform spherical shaped nanoparticles with size ranging from 44 to 57 nm. The direct and indirect energy band gaps are calculated as 3.2 and 2.7 eV respectively. Functional groups presented in the compound were further investigated by FTIR, which are in good agreement with the previous studies.

(Received November 10, 2016; Accepted July 6, 2017)

*Keywords:*Tin mono sulfide, Nanoparticles, Optical properties, Environmentally safe material

1. Introduction

The solar cells are among environment friendly source of thermal and electrical energy. Developments of cost-effective and efficient material for solar cells have been an ongoing process for several decades[1-4]. In the field of optoelectronic devices crystalline silicon (c-Si), II-VI and III-V compound semiconductors have been a choice of researchers. Silicon however, is highly efficient but the processingis not cost effective, meanwhile the prominent alternates GaAs and CdTe are highly toxic and are discouraged being non-environment friendly materials.The arsenic compounds may cause irritation to skin and mucous membranes, leading to a permanent damage of these vital membranes of the human body, heart, liver, blood and vascular system, inducing other physiological imbalances leading towards cancer [5]. Yet the GaAs is far less toxic then CdTe for cadmium being exceedingly toxic element. Moreover, it is among the extremely stable crystalline compounds formed and one of the top six toxic and environmentally hazardous materials known so far. As if ingested or the dust is inhaled may become fatal, even if it is handled improperly i.e. without appropriate gloves and other lab safety precautions, it can become a source of intoxication, lesions, necrosisleading to cancer. The highly reactive surface of cadmium telluride quantum dots triggers extensive reactive oxygen damage to the cell membrane, mitochondria, and cell nucleus leading to a number of malfunctions, diseases and spontaneous mutation[6]. In addition, the cadmium telluride films are typically recrystallized in a toxic compound of cadmium chloride which becomes a serious environmental hazard based on its solubility.

In-order to overcome these problems, sulfosalts provides a better replacement due to their nontoxic nature and low cost [7,8].Most of the metal sulfides are generally insoluble and hence

*Corresponding author: asad.ghufran@iiu.edu.pk

based on non-bioavailability, have little toxic action towards the interruption of biological processes within organisms and in the environment. For one exception of SnS through the liberation of hydrogen sulfide fumes/gas, besides H_2S fumes inhalation of tin dusts over a period of years may cause damage to respiratory system and lead to pneumoconiosis [9]. These properties make them a better alternative absorber material for photovoltaic applications. Recent investigations on new photovoltaic materials have been of considerable interest and researchers are investigating for understanding and engineering the properties of SnS thin films for photovoltaic applications [5-8,13]. Tin mono sulfide (SnS) is IV-VI binary semiconductor compound; both tin and sulfur are abundant elements. The SnS has p-type conductivity with orthorhombic structure with both direct and indirect band gap values 1.3–1.5 eV and 1.0–1.1 eV, respectively. It has higher absorption coefficient (~$10^5 cm^{-1}$) as compared to GaAs and CdTe.

We have studied the physical properties of SnS nanoparticles prepared by co-precipitation method. Tin mono sulfide have a variety of applications in optoelectronic devices, biotechnology and biomedicines etc. [10-13]. In order to fabricate nanoparticles, different synthesizing methods are used such as co-precipitation method, electrodeposition and chemical bath deposition etc. [14]. The simplest and cost effective method is the precipitation method [15]. We have applied a new and different chemical route in this method which is simple and cost effective for the formation of SnS nanoparticles. The prepared SnS nanoparticles can be coated on a conducting glass substrate to form thin layer for the applications as absorber layer in solar cell [16]. Apart from the synthesis, the structural, surface morphological and optical properties have been investigated.

To the best of present knowledge besides a lot of work on the photolytic properties of the SnS, chemical, physical and toxicological properties of tin sulfide (SnS) have not been thoroughly investigated and recorded.

2. Experimental

2.1 Synthesis of SnS Nanoparticles

The SnS nanoparticles were prepared by precipitation method. All the chemicals were of analytical reagent grade obtained from Sigma Aldrich and used without any further purification. 5.34 gram of tin powder and 0.721 gram of sulfur powder were mixed with paraffin oil (45 ml) in a round bottom flask. The solution was stirred for about 20 hours at constant temperature of 250ºC, and immediately transferred to centrifuge tubes to cool down to room temperature, and finally centrifuged at 4000 rpm for 10 minutes. The separated particles were washed three times with chloroform and dried at 80ºC for 5 hours. Finally, the product in black color was obtained. The whole synthesis process is summarized as flow chart given in Fig. 1.

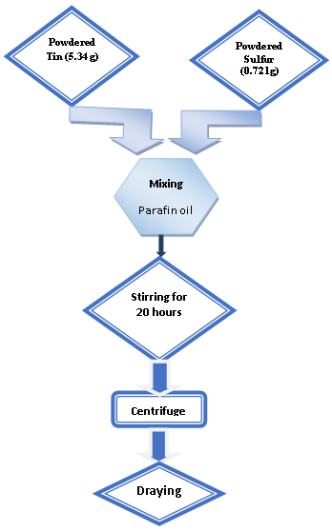

Fig 1 The flow chart for synthesis of SnS nanoparticles

3. Results and discussions

The structural analysis including phase, particle size and lattice strain were determined by the XRD data. The surface morphology and size of nanoparticles were investigated by scanning electron microscope (SEM). The elemental composition of SnS nanoparticles was determined by Energy Dispersive X-ray Spectroscopy (EDS). The optoelectronic property such as optical band gap was determined by Diffuse Reflectance Spectroscopy (DRS). Fourier transform infrared spectroscopy (FTIR) was used to see the functional groups and absorption of nanoparticles.

3.1 Structural Properties

XRD analysis was used to examine the crystal structure and plane orientation of SnS nanoparticles. Fig. 2 shows the diffraction patterns of SnS nanoparticles. The lattice spacing was calculated by Bragg's reflection.

$$d = \frac{\lambda}{(2Sin\theta)} \tag{1}$$

where θ is the angle between normal to diffraction plane of incident X-ray, λ is the wavelength, which is in our case was Cu-Kα radiation at 1.54 Å. The calculated d-spacing was 2.8 Å. The peaks were identified by using X`Pert High Score software, all the diffraction peaks are indexed to orthorhombic phase of SnS and calculated by the following relation

$$\frac{1}{d^2} = \frac{h^2}{a^2} + \frac{k^2}{b^2} + \frac{l^2}{c^2} \tag{2}$$

The calculated lattice parameters for sample is a = 2.334Å, b = 11.2Å, c = 3.985Å. This is in good agreement with the values of standard card (JCPDS No. 00-001-0984-1375), in Fig. 2, different peaks are observed at the diffraction angles of 22º, 26º, 27.5º, 30º, 31.5º, 32º, 39º, 42.5º, 44.6º, 45.5º, 50.5º, 51.2º, 53.1º, 54.2º, 56.6º with corresponding miller indices (110), (120), (021), (101), (111), (040), (131), (210), (141), (002), (211), (151), (122), (061) and (042). In addition to SnS peaks, two peaks with low intensities were observed in XRD pattern which are labeled and indexed to the of β-Sn phase (JCPDS No. 00-001-0926). The average crystallite size has been calculated by Debye Scherrer's formula [17,18].

$$t = \frac{k\lambda}{\beta Cos\theta} \tag{3}$$

Where t is the particle size, k is Scherrer`s constant equal to 0.9, λ is X-ray wavelength, β is full width at half maxima and θ is braggs angle in radian. The average particle size was calculated as 48.44nm.

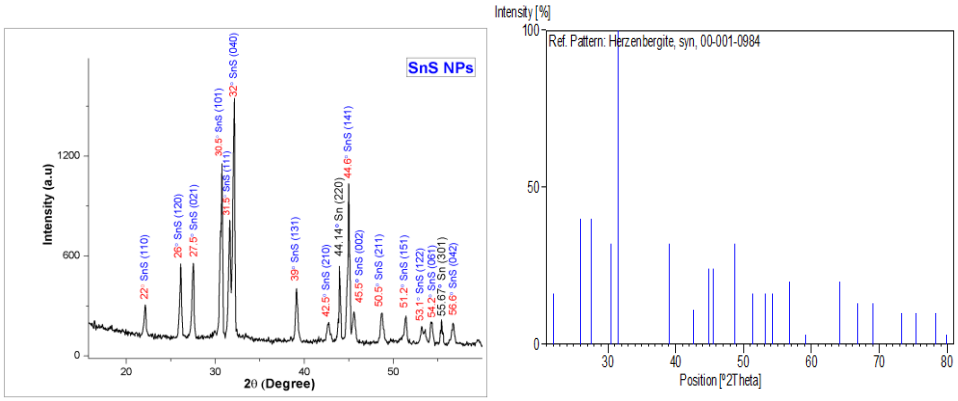

a) Diffraction pattern of SnS *b) Reference pattern of SnS*

Fig. 2 XRD patterns of SnS nanoparticles.

3.2 Surface morphology

The surface morphology and the grain size were determined by using scanning electron microscope (SEM). Fig. 3 shows the SEM image of as prepared nanoparticles. It can be clearly seen that the particles are spherical in shape with different size distribution, averaging more than 10 particles gives size of 50 nm ± 10 nm.

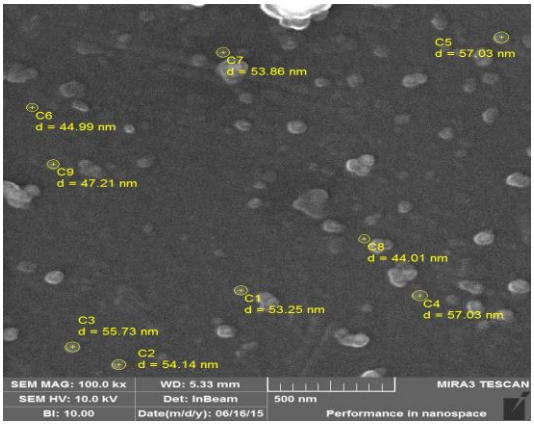

Fig. 3. SEM image of SnS nanoparticles.

3.3 Compositional Analysis

Elemental composition was determined using computer controlled digital scanning electron microscope attached with the EDX system of SnS nanoparticles. The S to Sn atomic % ratio is 1.53. The same ratio was also observed by other researchers [19]. Elemental composition of nanoparticles is summarized in Table 1.

Table 1 Elemental composition of SnS nanoparticles.

Elements	Weight %	Atomic %
Tin	53.17	16.60
Sulphur	21.59	24.95
Oxygen	25.24	58.45

Fig. 4 shows the EDS spectrum of SnS nanoparticles where the peaks of tin and sulfur are clearly seen. A small peak showing some amount of oxygen was also observed, probably due to presence of oxygen during drying process. No other impurity was found.

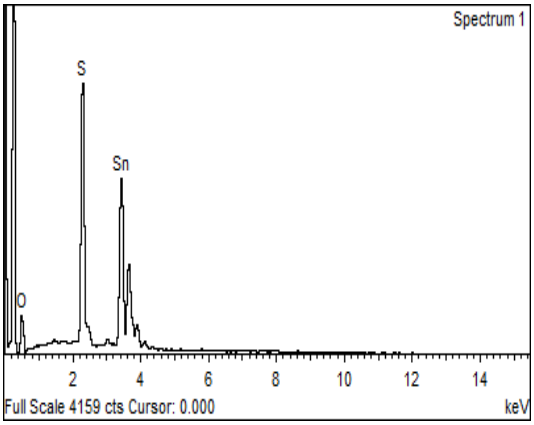

Fig. 4: EDX spectrum of SnS nanoparticles

3.4 Optical Properties

Diffuse reflectance spectroscopy (DRS) was used to determine the energy band gap of SnS nanoparticles. The DRS spectra is shown in Fig. 5. The graph shows decreasing as a function of reflectance with increasing wavelength. We can see that the reflectance is reaching to its lowest in the visible region from 300 to 800 nm making this material extremely useful as absorber layer for solar cell.

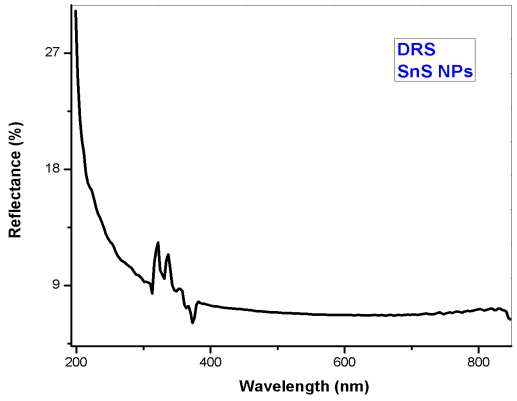

Fig. 5: DRS spectra of SnS nanoparticles.

The energy band gap is also measured by DRS spectra in UV-visible range. The obtained reflectance spectra are shown in Fig. 4, and the measurement parameters are shown in Table 2.

Table 2 DRS Analysis Parameters

Sr. No.	Measurement Conditions	
1	Measurement Wavelength Range	200 to 800 nm
2	Scan Speed	Medium
3	Sampling Pitch	1.0 nm
4	Photometric Value	Reflectance
5	Slit Width	(20) nm
6	Grating Switching Wavelength	720 nm
7	Detector Switching Wavelength	830 nm

The absorption edge occurs at different wavelengths for different materials. The reduction in the reflectance spectrum at specific wavelength gives information about the optical band gap. According to the Tauc Relation[20,21]

$$(h\nu\alpha)^n = A(h\nu - E_g) \quad (2)$$

where h is Planck's constant, ν is frequency of vibration, α represents absorption coefficient; A is proportional constant and E_g is band gap, and The Kubelka-Munk function for any wavelength is given by

$$\alpha = F(R_\infty) = \frac{(1-R)^2}{2R} \quad (3)$$

The value of the exponent n in equation 2, denotes the nature of the sample transition. The values of n are 2, ½, 3. 3/2 for indirect allowed, direct allowed, indirect forbidden and direct forbidden transitions respectively. For our material, only two, i.e. direct and indirect transition are allowed. The obtained DRS is converted to Kubelka-Munk function (KB), on the vertical axis quantity $F(R_\infty)$, which is proportional to the α. Using the Kubelka-Munk function, the $\{h\nu * F(R\infty)\}^n$ was plotted as a function of hν. The curve that plots the value of $(h\nu - (h\nu F(R\infty))^2)$ and the

respective tangent on the horizontal axis hν and vertical axis $(h\nu F(R\infty))^2$ is drawn. Here, the unit for hν is electron volts (eV), and its relationship to the wavelength
λ (nm) becomes

$$h\nu = 1239.7/\lambda. \quad (4)$$

A tangent is drawn to the point of inflection on the curve and the hν value at the point of intersection with the horizontal axis determines the energy band gap. The direct and indirect band gap of SnS nanoparticles is shown in Fig. 5 and 6 respectively. The calculated direct band gap is 3.2 eV, whereas indirect band gap is 2.5 eV.

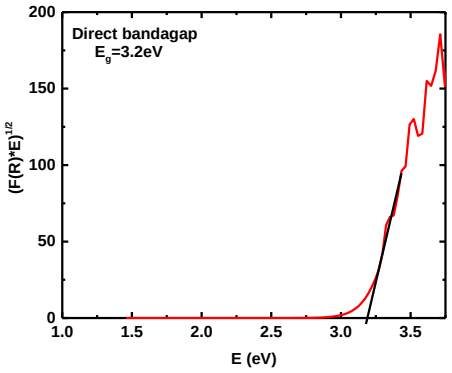

Fig. 5 Direct band gap of SnS nanoparticles.

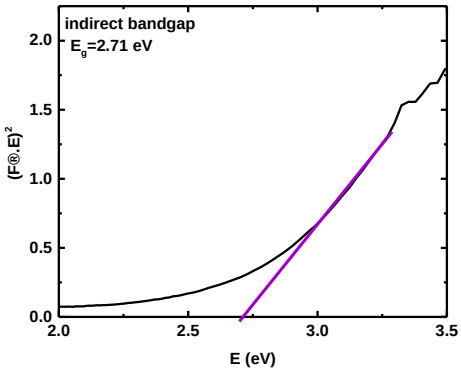

Fig. 6 Indirect band gap of SnS nanoparticles.

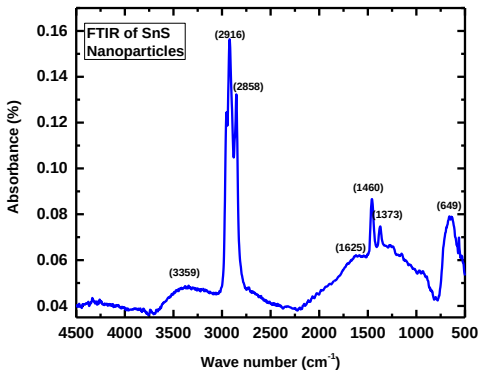

Fig. 7. FTIR absorption spectrum of SnS nanoparticles

The peaks at 647, 1000-1200, 1371, 1460 cm^{-1} correspond to SnS nanoparticles and broad valley at 750-950 and 2350 cm^{-1} are the absorption of SnS and hydroxyl group. Besides the SnS vibration, it can be seen from Fig. 7 that a significant absorption at 3,359 cm^{-1} (broad peak at 3200-3550 cm^{-1}) with a shoulder, are due to the strong OH stretching vibrations. The weak band near 1625 cm^{-1} is assigned to H–O–H bending vibrations mode probably due to the adsorption of water at the time of sample preparation. The FTIR findings are summarized in Table 2.

Table2: Modes for SnS nanoparticles

Sr. No	Wavenumber (cm^{-1})	Functional group
1	647,1000-1200 1373, 1460	SnS
2	750-950, 2350	SnS + hydroxyl group
4	3100-3550	OH stretching

4. Conclusions

Tin sulfide nanoparticles were synthesized successfully by co-precipitation method. The XRD analysis showed that the particles have orthorhombic crystal structure. The particle size was estimated by Debye-Scherrer formula as 48.44 nm, which has been confirmed by SEM analysis. The atomic percentage for S to Sn was 1.53 was determined by EDS. In DRS spectra the reflection decreases as a function of wavelength in the visible region making this material favorable candidate as absorber layer for solar cell.

The optical direct and indirect band gap calculated by Kubelka-Munk function is about 3.2 eV and 2.7 eV respectively. Compared to direct band gap 1.3 eV and indirect band gap 1.09 eV in bulk SnS, both direct transition and indirect transition in nanoparticles show an obvious quantum-size effect, which is on the higher side of the bulk band gap value, possibly arising from reduction of particle size. Deviation of stoichiometry may also have contributed to enhanced band gap. The strong peaks in the FTIR spectrum at 647 and 2360 cm^{-1}also confirm the presence of SnS nanoparticles.

Acknowledgement

WAAS, WHS, MAG and NR are thankful to the graduate students H. Qureshi and M. Zaman for their hard working to complete the research project.

WAAS would like to thank Dr. Nazar Abbas Shah of COMSATS, Islamabad for fruitful discussion on this subject.

References

[1] J. B. Li, V. Chawla, B. M. Clemens, Advanced Materials **24**, 720 (2012).
[2] P. P. Choi, O. C. Miredin, and R. Wuerz, Surf. Interface Anal. **44**, 1386 (2012).
[3] J. J. Scragg, P. J. Dale, D. Colombara, L. M. Peter ChemPhysChem. **13**, 3035 (2012).
[4] L. Grenet, S. Bernardi, D. Kohen, C. Lepoittevin, S. Noel, N. Karst, A. Brioude, S. Perraud, H. Mariette, Solar Energy Mater. & Solar Cells, **101**, 11 (2012).
[5] A. Tanaka Toxicity of indium arsenide, gallium arsenide, and aluminum gallium arsenide. Toxicology and applied pharmacology, **198**(3), 405 (2004).
[6] J. B.Johnson, H.Jones, B. S.Latham, J. D.Parker, R. D.Engelken, C. Barber, Semiconductor Science and Technology**14**(6), 501(1999).
[7] Ahmed Saeed,Nisar Ali, Waqar A. A. Syed, Chalcogenide Letters **10**(4), 143 (2013).

[8] Ying Xu,Najeh Al-Salim, Richard D.Tilley,Nanomaterials **2**, 54(2012)
[9] D. L.Morgan, C. J.Shines, S. P.Jeter, M. E.Blazka, M. R.Elwell, R. E.Wilson,P. D. Moskowitz,Toxicology and applied pharmacology, **147**(2), 399(1997).
[10] U. Simon, R. Flesch, H. Wiggers, G. Schon, G. Schmid, J. Mater. Chem. **8**, 517(1998),
[11] D.Mrinmoy,S. G.Partha, M. R. Vincent, Advanced Materials, **20**, 4225(2008).
[12] Y.Wang, Z.Tang, N. A. Kotov, Materials Today **2005**(8), 20(2005).
[13] L.Shi, Y.Xu, S.Hark, Y.Liu, S.Wang, L.-M.Peng, K.Wong, Q. Li, Nano Letters**7**, 3559(2007).
[14] D. Avellaneda,B. Krishnan,T.K.Da Roy,ApplPhys A**3**, 156(2012).
[15] MeriemReghima,AnisAkkari, CathyGuasch, Michel Astagne, NajouaKamoun-Turki journal of renewable and sustainable energy **5**, 6778(2013).
[16] M. Pal, A. Martinez Ayala, N.R. Mathews, X. Mathew, Journal of Nano Research, **28**, 91 (2014).
[17] P. Scherrer, Nachrichten von der Gesellschaft der Wissenschaftenzu Göttingen, Mathematisch-PhysikalischeKlasse**2**, 98 (1918).
[18] A.Patterson, Phys. Rev. **56**(10) 978(1939).
[19] M. Devika, K. T. Ramakrishna Reddy, N. Koteeswara Reddy, K. Ramesh, R. Ganesan, E. S. R. Gopal, K. R. Gunasekhar J. Appl. Phys. **100**, 0235(2006).
[20] A.A. Al-Ghamdi, S.A. Khan, S. Al-Heniti, F.A. Al-Agel, T. Al- Harbi, M. Zulfequar J. Alloys Compd. **505**, 229(2010).
[21] S.A. Khan, J.K. Lal, A.A. Al-Ghamdi Optics & Laser Technology **42**(5), 839(2010).